

An adaptive high order direct solution technique for elliptic boundary value problems

A. Gillman and P. Geldermans

Department of Computational and Applied Mathematics, Rice University

Abstract: This manuscript presents an adaptive high order discretization technique for elliptic boundary value problems. The technique is applied to an update version of the Hierarchical Poincaré-Steklov (HPS) method. Roughly speaking, the HPS method is based local pseudospectral discretizations glued together with Poincaré-Steklov operators. The new version uses a modified tensor product basis which is more efficient and stable than previous versions. The adaptive technique exploits the tensor product nature of the basis functions to create a criterion for determining the parts of the domain that require additional refinement. The resulting discretization achieves the user prescribed accuracy and comes with an efficient direct solver. The direct solver increases the range of applicability to time dependent problems where the cost of solving elliptic problems previously limited the use of implicit time stepping schemes.

1. INTRODUCTION

This manuscript presents an adaptive discretization technique for problems of the form

$$(1) \quad \begin{cases} Au(\mathbf{x}) = g(\mathbf{x}) & \mathbf{x} \in \Omega, \\ u(\mathbf{x}) = f(\mathbf{x}) & \mathbf{x} \in \Gamma = \partial\Omega, \end{cases}$$

where Ω is a rectangle in \mathbb{R}^2 with boundary Γ , and where A is a coercive elliptic partial differential operator

$$(2) \quad [Au](\mathbf{x}) = -c_{11}(\mathbf{x})[\partial_1^2 u](\mathbf{x}) - 2c_{12}(\mathbf{x})[\partial_1 \partial_2 u](\mathbf{x}) - c_{22}(\mathbf{x})[\partial_2^2 u](\mathbf{x}) \\ + c_1(\mathbf{x})[\partial_1 u](\mathbf{x}) + c_2(\mathbf{x})[\partial_2 u](\mathbf{x}) + c(\mathbf{x})u(\mathbf{x}).$$

The discretization technique presented here is an updated version of the composite spectral discretization techniques presented in [5, 4, 7]. It is based on local pseudospectral discretizations that are “glued” together by Poincaré-Steklov operators. A direct solver is constructed by hierarchically gluing the Poincaré-Steklov operators together. Hence, the discretization technique is called the Hierarchical Poincaré-Steklov (HPS) method. The adaptive refinement strategy presented in this manuscript is inspired by the technique in [6] which uses the Chebychev expansion coefficients of the local approximate solution to develop a refinement strategy. Like the HPS methods in [5, 4, 7, 2], the adaptive discretization technique can also be modified to handle a range of different domains, including curved ones. For problems with smooth coefficients, we demonstrate that the adaptive strategy easily identifies the regions requiring refinement and achieves at least the user specified accuracy (up to the nine digit limit of pseudospectral discretizations). For problems with non-smooth coefficients the adaptive technique achieves the same accuracy as the uniform refinement scheme. Additional novelty of this paper lies in an update to the local discretization which reduces the computational cost of the method.

While constructing the adaptive discretization and the direct solver has a computational cost that scales $O(N^{3/2})$ where N is the number of discretization points, the cost of applying the solver is $O(N \log N)$ with a small constant. The constant in the solve step is typically much smaller than for a uniform discretization thus making the method useful for applications that involve *many* elliptic solves that require locally refined high order discretizations. For example, having an efficient direct solver for elliptic partial differential equations can increase the range of problems for which implicit time stepping schemes are computationally affordable.

1.1. Overview of discretization technique. Roughly speaking the adaptive discretization technique can be broken into three steps.

- Step 1: First, the geometry is partitioned into a collection of patches using an quad tree with an adaptive interpolation strategy applied so that the coefficients in (2) and body load function $g(\mathbf{x})$ in (1) are captured to the user prescribed tolerance ϵ .
- Step 2: Next each patch is discretized using a high order spectral collocation technique and the patches are “glued” together at the boundaries via a Poincaré-Steklov operators in a hierarchical fashion. In the process of gluing patches together, solution operators that propagate boundary data to the interior of a box are constructed. Then by applying the solution operators (small matrix vector multiplies) the boundary data is propagated down the hierarchical tree giving an approximate solution on each patch.
- Step 3: All patches are checked to see if they need to be further refined. If there are patches marked for refinement, they are refined and steps 2 and 3 are repeated until no patches are marked for refinement. If the refinement is localized in the domain, the bulk of the computation from step 2 can be reused.

While the method can be employed with any Poincaré-Steklov operator, for simplicity of presentation, this paper uses the Dirichlet-to-Neumann operator for gluing boxes as in [5, 7, 2]. For the Helmholtz experiments in this paper, the impedance-to-impedance (ItI) operator is used instead. [4] presents the ItI version of the solution technique for a homogeneous PDE. The appendix of this manuscript presents the ItI based solution technique when there is a body load $g(\mathbf{x})$.

In the previous versions of the HPS method special care was taken to deal with or avoid discretization points at the corners of the small patches. The method presented in [7] involves tedious bookkeeping of corner points. Additionally, possible singularities at the corners of the geometry Ω are of concern. By introducing interpolation at the level of the local discretizations, the methods in [5, 2, 4] avoid the corners of Ω . The new local discretization presented in this manuscript does not involve the corner points at all; thus improving the robustness and efficiency of the method.

For simplicity of presentation, the algorithms are described for a PDE with no body load (i.e. $g(\mathbf{x}) = 0$ in (1)). The manuscript begins by reviewing the HPS method with uniform refinement in section 2 but with the new local discretization technique. Next, the adaptive refinement procedure is presented in section 3. Then, numerical experiments demonstrating the performance of the method in section 4. Finally the manuscript concludes with a summary the paper in section 5.

2. THE HPS METHOD

This section presents the HPS method with a new local discretization technique. The HPS method begins by partitioning the domain Ω into a collection of square (or possibly rectangular) boxes, called *leaf boxes*. Throughout this paper, we assume that the parameter for the order of the discretization n_c is fixed ($n_c = 16$ is often a good choice). For a uniform discretization, the size of all leaf boxes is chosen so that any potential u of equation (1), as well as its first and second derivatives, can be accurately interpolated from their values at the local discretization points on any leaf box.

Next a binary tree on the collection of leaf boxes is constructed by hierarchically merging them, making sure that all boxes on the same level are roughly of the same size, cf. Figure 1. The boxes should be ordered so that if τ is a parent of a box σ , then $\tau < \sigma$. We also assume that the root of the tree (i.e. the full box Ω) has index $\tau = 1$. We let Ω_τ denote the domain associated with box τ . If a box ρ is child of σ and σ is a child of τ , we call ρ a *grandchild* of τ . For example in Figure 1, boxes 16 – 19 are grandchildren of box 4. (This vocabulary is needed for the adaptive scheme presented in section 3.)

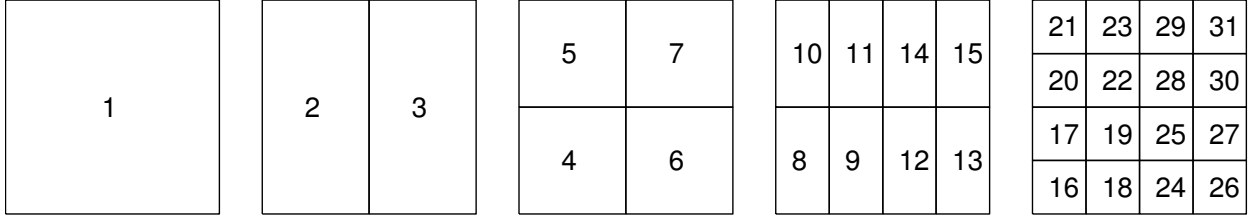


FIGURE 1. The square domain Ω is split into 4×4 leaf boxes. These are then gathered into a binary tree of successively larger boxes as described in Section 2. One possible enumeration of the boxes in the tree is shown, but note that the only restriction is that if box τ is the parent of box σ , then $\tau < \sigma$.

For each leaf box, approximate Dirichlet-to-Neumann (DtN) and solution operators are constructed via the *modified* spectral collocation method presented in section 2.1. The DtN approximations are “glued” together in a hierarchical fashion two boxes at a time. Section 2.2 presents the technique for constructing approximate DtN and solution operators for the union of two boxes. Algorithm 1 gives an overview of the construction of the discretization and direct solver. Once the hierarchical collection of approximate solution operators is constructed, the solution on the interior can be found for $O(N \log N)$ cost via Algorithm 2.

Definition 2.1 (Dirichlet-to-Neumann map). For domain Ω with boundary $\partial\Gamma$, the Dirichlet-to-Neumann (DtN) operator $T : H^1(\Gamma) \rightarrow L^2(\Gamma)$ is defined by

$$(3) \quad Tf = u_n,$$

for any $f(x) \in H^1(\Gamma)$, where u_n denotes the normal derivative of u on Γ in the direction of the normal vector n pointing out of Ω .

2.1. Leaf computation. This section describes a modified spectral collocation method for constructing approximate DtN \mathbf{T}^τ and solution Ψ^τ operators for a leaf box τ .

The modified spectral collocation technique begins with the classic $n_c \times n_c$ product Chebychev grid and the corresponding differential matrices \mathbf{D}_x and \mathbf{D}_y from for example [9]. Let I_i^τ denote the index vector corresponding to points on the interior of Ω^τ and I_b^τ denote the index vector corresponding to points on the boundary of Ω^τ **not** including the corner points based on the tensor classic tensor grid. Figure 2(a) illustrates the indexing of the points in terms of the classic discretization. Thus $\{\mathbf{x}_j\}_{j=1}^{n_c^2-4}$ denotes the discretization points in Ω^τ given by the union of the red and blue points in

Figure 2. We order the solution vector \mathbf{u} and flux vector \mathbf{v} according to the following: $\mathbf{u} = \begin{bmatrix} \mathbf{u}_b \\ \mathbf{u}_i \end{bmatrix}$

where \mathbf{u}_b and \mathbf{u}_i denote the approximate values of the solution on the boundary and the interior, respectively. The ordering of the entries related to the boundary corresponding to the discretization points is $I_b^\tau = [I_s, I_e, I_n, I_w]$ where I_s denotes the blue points on the bottom boundary in Figure 2, etc. Let $I^\tau = [I_b^\tau, I_i^\tau]$ denote the collection of all indices that are used in the discretization.

Thanks to the tensor product basis, we know the entries of \mathbf{D}_x and \mathbf{D}_y corresponding to the interaction of the corner points with the points on the interior of Ω^τ are zero. The directional basis functions for the other points on the boundary is not impacted by the removal of the corner points. Thus the differential operators from the classic pseudospectral discretization can be used to create the approximation of the local differential operator and DtN.

The classic discrete approximation of the differential operator on Ω^τ is given by

$$\mathbf{A} = -\mathbf{C}_{11}\mathbf{D}_x^2 - 2\mathbf{C}_{12}\mathbf{D}_x\mathbf{D}_y - \mathbf{C}_{22}\mathbf{D}_y^2 + \mathbf{C}_1\mathbf{D}_x + \mathbf{C}_2\mathbf{D}_y + \mathbf{C},$$

where \mathbf{C}_{11} is the diagonal matrix with diagonal entries $\{c_{11}(\mathbf{x}_k)\}_{k=1}^{n_c^2}$, and the other matrices \mathbf{C}_{ij} , \mathbf{C}_i , \mathbf{C} are defined analogously. Then the discretized differential equation on the new set of discretization

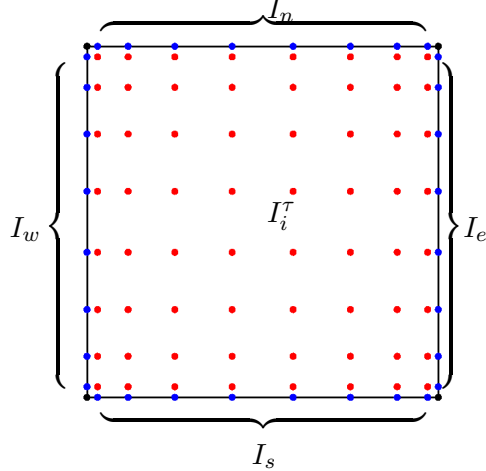


FIGURE 2. Illustration of the discretization points for a leaf box τ . The points in blue are the boundary points with indices $I_b^\tau = [I_s, I_e, I_n, I_w]$. The points in red are the interior points with indices I_i^τ . The points in black are the omitted corner points.

points is given by

$$\begin{bmatrix} \mathbf{I} & \mathbf{0} \\ \mathbf{A}_{i,i} & \mathbf{A}_{i,b} \end{bmatrix} \begin{bmatrix} \mathbf{u}_b \\ \mathbf{u}_i \end{bmatrix} = \begin{bmatrix} \hat{\mathbf{f}} \\ \mathbf{0} \end{bmatrix}$$

where $\mathbf{A}_{i,i} = \mathbf{A}(I_i^\tau, I_i^\tau)$, $\mathbf{A}_{i,b} = \mathbf{A}(I_i^\tau, I_b^\tau)$, and $\hat{\mathbf{f}}$ is fictitious Dirichlet boundary data.

When the boundary data is known, the approximate solution at the interior points is given by

$$(4) \quad \mathbf{u}_i = -\mathbf{A}_{i,i}^{-1} \mathbf{A}_{i,b} \mathbf{u}_b = \boldsymbol{\Psi}^\tau \mathbf{u}_b$$

where the matrix $\boldsymbol{\Psi}^\tau$ is the approximate solution operator.

Let \mathbf{L} denote the matrix made up of four block row matrices corresponding to taking the normal derivative of the basis functions on the leaf τ along each of the edges. In terms of the discrete operators \mathbf{L} is given by

$$\mathbf{L} = \begin{bmatrix} \mathbf{D}_x(I_s, I^\tau) \\ \mathbf{D}_y(I_e, I^\tau) \\ \mathbf{D}_x(I_n, I^\tau) \\ \mathbf{D}_y(I_w, I^\tau) \end{bmatrix}.$$

To construct the approximate DtN operator \mathbf{T}^τ , we take the normal derivative of the solution by applying \mathbf{L} to $\begin{bmatrix} \mathbf{I}_{4n_c-4} \\ \boldsymbol{\Psi}^\tau \end{bmatrix}$, i.e.

$$\mathbf{T}^\tau = \mathbf{L} \begin{bmatrix} \mathbf{I}_{4n_c-4} \\ \boldsymbol{\Psi}^\tau \end{bmatrix}$$

where \mathbf{I}_{4n_c-4} denotes the identity matrix of size $4n_c - 4$.

Remark 1. The classic tensor product discretization can be used to formulate the new discretization thanks to the separable basis (i.e. the corner points do not contribute the discretized differential equation). While interpolation along the edges without the corners is less accurate than if the corners were included, it is stable [1]. Since the discretization is run at high order (typically $n_c \geq 16$), a loss in accuracy is not observed in practice.

2.2. Merging two boxes. This section reviews of the procedure for constructing the DtN and solution matrices for the union of two boxes for which DtN matrices have already been constructed. More detailed descriptions are presented in [5, 7, 2].

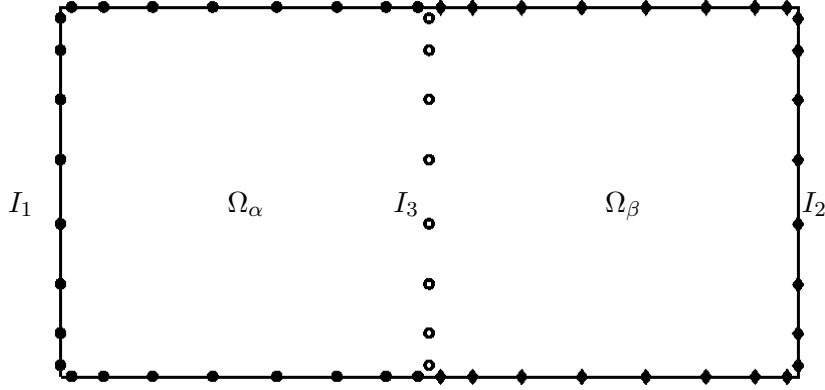


FIGURE 3. Notation for the merge operation described in Section 2.2. The rectangular domain Ω is formed by two squares Ω_α and Ω_β . The sets I_1 and I_2 form the exterior nodes (black), while I_3 consists of the interior nodes (white).

Let Ω_τ denote a box with children Ω_α and Ω_β so that

$$\Omega_\tau = \Omega_\alpha \cup \Omega_\beta.$$

For concreteness, let us assume that Ω_α and Ω_β share a vertical edge as shown in Figure 3. We partition the points on $\partial\Omega_\alpha$ and $\partial\Omega_\beta$ into three sets:

- I_1 Boundary nodes of Ω_α that are not boundary nodes of Ω_β .
- I_2 Boundary nodes of Ω_β that are not boundary nodes of Ω_α .
- I_3 Boundary nodes of both Ω_α and Ω_β that are *not* boundary nodes of the union box Ω_τ .

The indexing for the points on the interior and boundary of Ω^τ are $I_i^\tau = I_3$ and $I_b^\tau = [I_1, I_2]$, respectively.

Let u denote a solution to (1), with tabulated potential values \mathbf{u} and boundary fluxes \mathbf{v} . Ordering the DtN operators according to the J_k defined in Figure 3 results in the equations

$$(5) \quad \begin{bmatrix} \mathbf{v}_1 \\ \mathbf{v}_3 \end{bmatrix} = \begin{bmatrix} \mathbf{T}_{1,1}^\alpha & \mathbf{T}_{1,3}^\alpha \\ \mathbf{T}_{3,1}^\alpha & \mathbf{T}_{3,3}^\alpha \end{bmatrix} \begin{bmatrix} \mathbf{u}_1 \\ \mathbf{u}_3 \end{bmatrix}, \quad \text{and} \quad \begin{bmatrix} \mathbf{v}_2 \\ \mathbf{v}_3 \end{bmatrix} = \begin{bmatrix} \mathbf{T}_{2,2}^\beta & \mathbf{T}_{2,3}^\beta \\ \mathbf{T}_{3,2}^\beta & \mathbf{T}_{3,3}^\beta \end{bmatrix} \begin{bmatrix} \mathbf{u}_2 \\ \mathbf{u}_3 \end{bmatrix}.$$

Noting that \mathbf{v}_3 and the solution \mathbf{u}_3 is the same for each box (since the solution is smooth), the solution operator Ψ^τ is found by equating the bottom two row equations of (5);

$$(6) \quad \mathbf{u}_3 = (\mathbf{T}_{3,3}^\alpha - \mathbf{T}_{3,3}^\beta)^{-1} [-\mathbf{T}_{3,1}^\alpha \mid \mathbf{T}_{3,2}^\beta] \begin{bmatrix} \mathbf{u}_1 \\ \mathbf{u}_2 \end{bmatrix} = \Psi^\tau \begin{bmatrix} \mathbf{u}_1 \\ \mathbf{u}_2 \end{bmatrix}.$$

The operator Ψ^τ in (6) maps the solution on the boundary of Ω^τ to the solution \mathbf{u}_3 on the interior edge. The DtN operator is then constructed by plugging equation (6) into the top row equations in (5) and combining them to a matrix equation. The result is

$$(7) \quad \begin{bmatrix} \mathbf{v}_1 \\ \mathbf{v}_2 \end{bmatrix} = \mathbf{T}^\tau \begin{bmatrix} \mathbf{u}_1 \\ \mathbf{u}_2 \end{bmatrix}$$

where

$$(8) \quad \mathbf{T}^\tau = \begin{bmatrix} \mathbf{T}_{1,1}^\alpha & \mathbf{0} \\ \mathbf{0} & \mathbf{T}_{2,2}^\beta \end{bmatrix} + \begin{bmatrix} \mathbf{T}_{1,3}^\alpha \\ \mathbf{T}_{2,3}^\beta \end{bmatrix} (\mathbf{T}_{3,3}^\alpha - \mathbf{T}_{3,3}^\beta)^{-1} [-\mathbf{T}_{3,1}^\alpha \mid \mathbf{T}_{3,2}^\beta].$$

ALGORITHM 1 (build solution operators)

This algorithm builds the global Dirichlet-to-Neumann operator for (1).
 It also builds all the solution matrices Ψ^τ required for constructing an approximation to u at any interior point.
 It is assumed that if node τ is a parent of node σ , then $\tau < \sigma$.

-
- (1) **for** $\tau = N_{\text{boxes}}, N_{\text{boxes}} - 1, N_{\text{boxes}} - 2, \dots, 1$
 - (2) **if** (τ is a leaf)
 - (3) Construct \mathbf{T}^τ and Ψ^τ via the process described in Section 2.1.
 - (4) **else**
 - (5) Let σ_1 and σ_2 be the children of τ .
 - (6) Split $I_b^{\sigma_1}$ and $I_b^{\sigma_2}$ into vectors I_1, I_2 , and I_3 as shown in Figure 3.
 - (7) $\Psi^\tau = (\mathbf{T}_{3,3}^{\sigma_1} - \mathbf{T}_{3,3}^{\sigma_2})^{-1} [-\mathbf{T}_{3,1}^{\sigma_1} \mid \mathbf{T}_{3,2}^{\sigma_2}]$
 - (8) $\mathbf{T}^\tau = \begin{bmatrix} \mathbf{T}_{1,1}^{\sigma_1} & \mathbf{0} \\ \mathbf{0} & \mathbf{T}_{2,2}^{\sigma_2} \end{bmatrix} + \begin{bmatrix} \mathbf{T}_{1,3}^{\sigma_1} \\ \mathbf{T}_{2,3}^{\sigma_2} \end{bmatrix} \Psi^\tau$.
 - (9) Delete \mathbf{T}^{σ_1} and \mathbf{T}^{σ_2} .
 - (10) **end if**
 - (11) **end for**

ALGORITHM 2 (solve BVP once solution operator has been built)

This program constructs an approximation \mathbf{u} to the solution u of (1).
 It assumes that all matrices Ψ^τ have already been constructed in a pre-computation.
 It is assumed that if node τ is a parent of node σ , then $\tau < \sigma$.

-
- (1) $\mathbf{u}(k) = f(\mathbf{x}_k)$ for all $k \in I_b^1$.
 - (2) **for** $\tau = 1, 2, 3, \dots, N_{\text{boxes}}$
 - (3) **if** (τ is a parent)
 - (4) $\mathbf{u}(I_i^\tau) = \Psi^\tau \mathbf{u}(I_b^\tau)$.
 - (5) **end if**
 - (6) **end for**

3. ADAPTIVE DISCRETIZATION

This section presents an adaptive discretization technique for the boundary value problem (1) where the coefficient functions, right hand side and boundary data are smooth functions. As with the uniform discretization technique, the adaptive method produces a direct solver. The approximate solution obtained from the adaptive procedure is accurate (in the relative error) to a user prescribed tolerance ϵ .

The adaptive discretization technique has three major components.

- (1) Adaptive interpolation of the smooth coefficient functions in (1).
- (2) An algorithm for determining if a leaf box needs to be refined.
- (3) An efficient technique for constructing the direct solver for a refined mesh.

The first and last component are essential to making the adaptive procedure computationally feasible. To stop the refinement process, the method looks at the convergence relative error

$$E_{\text{rel}} = \frac{\|\mathbf{L}\mathbf{u}_{\text{coarse}} - \mathbf{u}_{\text{fine}}\|}{\|\mathbf{u}_{\text{fine}}\|}$$

where \mathbf{L} is a matrix that interpolates functions from the coarse discretization points to the fine discretization points. Algorithm 3 shows how these components fit together to construct the adaptive discretization technique. Section 3.1 presents the adaptive interpolation procedure for approximating a function $f(\mathbf{x})$ defined on Ω to a user prescribed tolerance ϵ . The section also presents the technique for merging two boxes that have a different number of leaf ancestors. Next section 3.2 presents the technique for deciding if a leaf box needs to be refined. Finally, section 3.3 explains an efficient technique for building the direct solver by reusing as much information as possible.

ALGORITHM 3 (Full adaptive procedure)

This algorithm builds an adaptive discretization and direct solver to solve (1) by making sure the approximate relative error E_{rel} is less than the user prescribed tolerance ϵ .

-
- (1) Construct a mesh which interpolates the smooth functions in equation (1) to ϵ accuracy.
 - (2) Build the direct solver from the interpolation mesh and compute $\mathbf{u}_{\text{coarse}}$.
 - (3) Set $E_{\text{rel}} = 1$
 - (4) **while** $E_{\text{rel}} > \epsilon$
 - (5) Use Algorithm 4 to pick which leaf boxes to refine.
 - (6) Update the solver (see section 3.3) and compute \mathbf{u}_{fine} .
 - (7) Compute approximate relative error $E_{\text{rel}} = \frac{\|\mathbf{L}\mathbf{u}_{\text{coarse}} - \mathbf{u}_{\text{fine}}\|}{\|\mathbf{u}_{\text{fine}}\|}$ where \mathbf{L} is an interpolation operator mapping the coarse to the fine grid.
 - (8) Set $\mathbf{u}_{\text{coarse}} = \mathbf{u}_{\text{fine}}$.
 - (9) **end while**

3.1. Adaptive interpolation. In order to keep the cost of the adaptive discretization as low as possible, we first create a mesh which allows for the smooth functions in (1) to be approximated with the local bases to the user prescribed tolerance ϵ . For simplicity of presentation, we describe the technique for interpolating a general smooth function $f(\mathbf{x})$ on Ω .

First, given n_c , a tensor product grid of n_c^2 Chebychev points is placed on Ω and each of its four grandchildren boxes (boxes 4, 5, 6 and 7 in Figure 1). Let $X^\Omega = \{\mathbf{x}_l^\Omega\}_{l=1}^{n_c^2}$ denote the set of interpolation points defined on box Ω . Likewise, let $X^j = \{\mathbf{x}_l^j\}_{l=1}^{n_c^2}$ for $j = 4, 5, 6,$ and 7 denote the set of interpolation points in box j . Set $X^{\text{grand}} = \bigcup_{j=4}^7 X^j$. Figure 4 illustrates the interpolation points on Ω and the four grandchildren when $n_c = 16$ and $\Omega = [0, 1]^2$.

Let \mathbf{f}^Ω denote the vector whose entries correspond to $f(\mathbf{x})$ evaluated at the points in X^Ω and \mathbf{L}_{etk} denote the interpolation operator which maps data from X^Ω to X^{grand} . (The notation etk stands for “elder to kids.”) Then $\mathbf{f}_{\text{app}} = \mathbf{L}_{\text{etk}}\mathbf{f}^\Omega$ is the approximate value of $f(\mathbf{x})$ at the points in X^{grand} interpolated from the values of $f(\mathbf{x})$ at the points in X^Ω . Let \mathbf{f}_{kids} denote the vector whose entries correspond to $f(\mathbf{x})$ evaluated at the points in X^{grand} . If the relative error $E_{\text{interp}} = \frac{\|\mathbf{f}_{\text{kids}} - \mathbf{f}_{\text{app}}\|}{\|\mathbf{f}_{\text{kids}}\|}$ is greater than ϵ , Ω is split into the four grandchildren boxes. The process is repeated until the local interpolation on all of the leaf boxes can approximate $f(\mathbf{x})$ to the user prescribed tolerance ϵ .

To merge boxes on different levels, the operators on the shared edge need to be interpolated to correspond to the evaluation at the same points as presented in section 3.1.1. To maintain stability of this interpolation, we utilize a level restricted tree which requires neighboring leaf boxes to be no more than two times bigger than each other. Figure 5 (a) illustrates the mesh from the adaptive

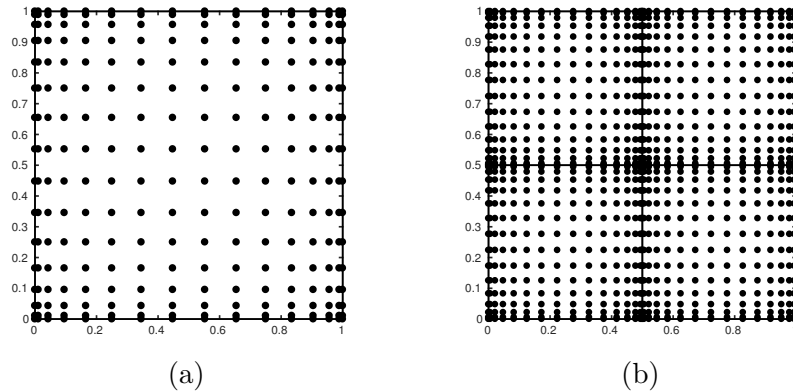


FIGURE 4. Illustration of the interpolation points on (a) $\Omega = [0, 1]^2$ and (b) its four grandchildren.

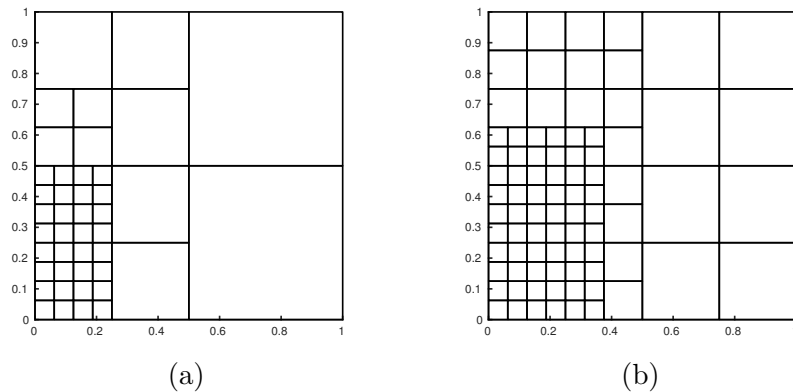


FIGURE 5. Illustration of the mesh resulting from adaptive interpolation applied to $f(\mathbf{x}) = f(x, y) = e^{-(1000(x-0.11)^2+100(y-0.27)^2)}$ (a) without and (b) with level restriction. The tolerance was set to $\epsilon = 1e - 6$.

interpolation applied to

$$f(\mathbf{x}) = f(x, y) = e^{-(1000(x-0.11)^2+100(y-0.27)^2)}$$

on $\Omega = (0, 1)^2$ with $n_c = 16$ and $\epsilon = 1e - 6$. Figure 5 (b) illustrates the mesh after level restriction is enforced.

3.1.1. Merging two boxes on different levels. After the initial mesh is generated, the HPS solver needs to be constructed. Since the mesh is not uniform, the merge procedure needs to be modified to handle the unstructured mesh. The key difference is that boxes will be merged which do not have the same number of discretization points on the shared edge. This section presents a technique for merging two such boxes.

For simplicity of presentation, we present the technique for merging a leaf box α with a box β whose grandchildren are leaf boxes. In this situation, Ω^β has twice as many points on its boundary as Ω^α . Likewise, the DtN matrix \mathbf{T}^β is twice the size as \mathbf{T}^α . Figure 6 illustrates discretization points on the two boxes. The points in I_3 from box α do not match the points in I_3 from box β . To make it so we can merge the two boxes, we use interpolation. Let \mathbf{L}_{2t1} and \mathbf{L}_{1t2} denote the interpolation operators that map two panels to one panel on the same interval and vice versa. Then the solution and DtN matrices on $\Omega^\tau = \Omega^\alpha \cup \Omega^\beta$ are given by inserting the interpolation operators

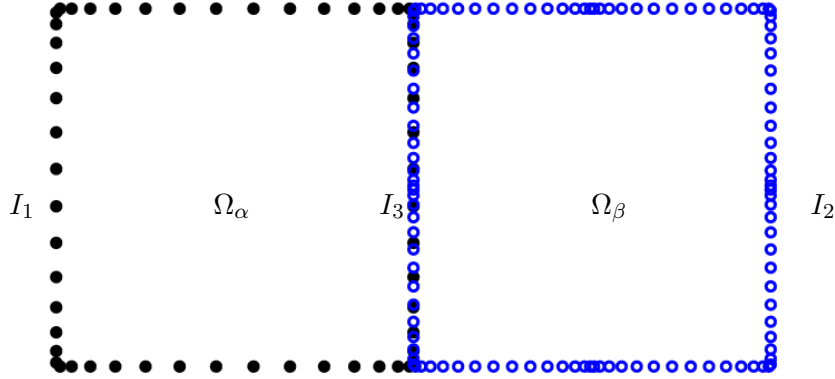


FIGURE 6. Notation for the merge operation when boxes are on different levels as described in Section 3.1.1. The rectangular domain Ω is formed by two squares Ω_α and Ω_β . The points on the boundary of Ω_α are solid black dots while the points on the boundary of the children of Ω_β are blue hollow dots.

into the appropriate locations in equations (6) and (7);

$$\Psi^\tau = (\mathbf{T}_{3,3}^\alpha - \mathbf{L}_{2t1} \mathbf{T}_{3,3}^\beta \mathbf{L}_{1t2})^{-1} [-\mathbf{T}_{3,1}^\alpha \mid \mathbf{L}_{2t1} \mathbf{T}_{3,2}^\beta]$$

and

$$\mathbf{T}^\tau = \begin{bmatrix} \mathbf{T}_{1,1}^\alpha & \mathbf{0} \\ \mathbf{0} & \mathbf{T}_{2,2}^\beta \end{bmatrix} + \begin{bmatrix} \mathbf{T}_{1,3}^\alpha \\ \mathbf{T}_{2,3}^\beta \mathbf{L}_{1t2} \end{bmatrix} \Psi^\tau.$$

Remark 2. Merging two boxes on different levels was also presented in [2]. There the DtN operator \mathbf{T}^β is interpolated to one corresponding an operator so that the number of points per edge matches the operator on box α . The method presented in this paper does not take this approach the coarse sampling of boundary data on Ω^1 may not sufficient resulting in a loss of accuracy.

3.2. Adaptive PDE discretization. This section describes the adaptive discretization technique which exploits the fact that the local basis is a Chebychev tensor product basis. The technique is inspired by [6] where a decay condition on the local Chebychev expansion coefficients was used to build an adaptive discretization technique for one dimensional integral equations. Recall that for one dimensional interpolation that the Lagrange interpolant through Chebychev points can be expressed as a partial Chebychev expansion with coefficients that can be found via the Fast Fourier Transform (FFT)[3]. Since each leaf box has a modified tensor product basis, we look at the directional Chebychev coefficients to build a refinement criterion.

Specifically, for a leaf box Ω^τ , let $\{x_j\}_{j=1}^{n_c}$ and $\{y_j\}_{j=1}^{n_c}$ denote the one dimensional Chebychev interpolation points that the x and y coordinates any discretization point can take on. For a fixed x_j , $j = 2, \dots, n_c - 1$, let B_j denote the Chebychev coefficients in the y -direction. Then let

$$S_y = \max_{j=2, \dots, n_c-1} (|B_j(n_c - 1)| + |B_j(n_c) - B_j(n_c - 2)|)$$

be an indicator of the decay of the coefficients in the y -direction. Likewise for a fixed y_j , $j = 2, \dots, n_c - 1$, let B_j denote the Chebychev coefficients in the x -direction and

$$S_x = \max_{j=2, \dots, n_c-1} (|B_j(n_c - 1)| + |B_j(n_c) - B_j(n_c - 2)|)$$

be an indicator of the decay of the coefficients in the x -direction. Then, for each leaf box τ , we define $S_\tau = \max\{S_x, S_y\}$. Let

$$S_{\text{div}} = \frac{\max_{\text{leaf boxes } \tau} S_\tau}{4}.$$

Then any leaf box τ which has $S_\tau > S_{\text{div}}$ is marked for further refinement. Algorithm 4 presents a pseudocode for determining which leaf boxes need refinement.

Remark 3. As with the adaptive interpolation technique, level restriction is enforced.

ALGORITHM 4 (Adaptive discretization)

This algorithm creates an adaptive mesh and a direct solver for approximating solutions to (1) to a user specified tolerance ϵ . It assumes a tree structured mesh and the corresponding direct solver are given.

```

(1) for  $\tau = N_{\text{boxes}}, N_{\text{boxes}} - 1, N_{\text{boxes}} - 2, \dots, 1$ 
(2)   if ( $\tau$  is a leaf)
(3)     for  $j = 2, \dots, n_c - 1$ 
(4)       Let  $B_j$  denote the y-directional Chebychev coefficients with fixed  $x_j$ 
           of the approximate solution on  $\tau$ .
(5)     end for
(6)     Let  $S_y = \max_{j=2, \dots, n_c-1} (|B_j(n_c - 1)| + |B_j(n_c) - B_j(n_c - 2)|)$ 
(7)     for  $j = 2, \dots, n_c - 1$ 
(8)       Let  $B_j$  denote the x-directional Chebychev coefficients with fixed  $y_j$ 
           of the approximate solution on  $\tau$ .
(9)     end for
(10)    Let  $S_x = \max_{j=2, \dots, n_c-1} (|B_j(n_c - 1)| + |B_j(n_c) - B_j(n_c - 2)|)$ 
(11)    Let  $S_\tau = \max\{S_x, S_y\}$ 
(12)  end if
(13) end for
(15) for  $\tau = N_{\text{boxes}}, N_{\text{boxes}} - 1, N_{\text{boxes}} - 2, \dots, 1$ 
(16)   if ( $\tau$  is a leaf)
(17)     if  $S_\tau > S_{\text{div}}$ 
(18)       Add  $\tau$  to the refinement list.
(19)     end if
(20)   end for
(21) Update the solver using the method in Section 3.3.
```

3.3. Updating the solver. Once the list of leaf boxes marked for refinement is made, we need to solve (1) with the refined grid to determine. Constructing the direct solver from scratch is computationally expensive and unnecessary when the refinement is localized. This section presents a technique for building the solver for the refined mesh while making use of the existing solver. The key observation is the fact that the solution technique is naturally domain decomposing. This means that the only parts of the solver that need to be modified are the parts that touch the refined regions.

The first step in this process is to make a list of all boxes affected by the local refinement. To do this, starting from the list of boxes refined, we sweep the binary tree making note of all the ancestors affected. For example, if boxes 16, and 18 were the only boxes marked for refinement in Figure 1, the solver would need to update the operators for boxes 1, 2, 4, 8 and 9. The operators for the other boxes need not be touched.

Next DtN and solution matrices are constructed by moving from through the list of effected boxes starting from the bottom of the tree (i.e. first processing the leaf boxes then its ancestors in order of ancestor).

Remark 4. Further acceleration can be gained by creating new tree structures based on the refinement regions. For the example where boxes 16 and 18 in Figure 1 require refinement, DtN and solution matrices can be constructed for the union of boxes 5, 6, 7, 17 and 19. Then the computation is limited to the boxes 16, 18, their union and gluing the union with the remainder of the geometry. For the problems under consideration in this manuscript, this technique was not employed.

4. NUMERICAL RESULTS

This section illustrates the performance of the adaptive discretization technique for a collection of problems. First, in section 4.1, three problems suggested in [8] to test adaptive discretization techniques for elliptic PDEs are considered. For each of these problems the solution is known but each poses a different challenge for adaptive discretization techniques. Section 4.2 considers low- to mid-frequency Helmholtz problems where the wave speed has sharp and smoothly varying contrast with a Gaussian source term. The solution to these problems is unknown. The globally oscillatory nature of the solution adds to the challenge of accurately discretizing these problems.

For two choices of discretization order ($n_c = 8$ and $n_c = 16$), the following quantities are reported.

N_i : the number of leaf boxes after adaptive interpolation

N_f : the number of leaf boxes after adaptive discretization

E_{rel} : the average relative error (or relative convergence error) over all the leaf boxes

4.1. Problems with known solutions. This section reports the performance of the solution technique for three problems where the solution is known and the partial differential equation has smooth coefficients on the domain $\Omega = (0, 1)^2$. The problems under consideration are the following:
Boundary layer: The Dirichlet boundary value problem

$$-\alpha \nabla^2 u + 2 \frac{\partial u}{\partial x} + \frac{\partial u}{\partial y} = f(x, y),$$

where the solution is given by

$$u(x, y) = (1 - e^{-(1-x)/\alpha})(1 - e^{-(1-y)/\alpha}) \cos(\pi(x + y))$$

and the parameter $\alpha = 10^{-3}$ determines the steepness of the boundary layer.

Locally oscillatory solution: The Dirichlet boundary value problem

$$-\nabla^2 u - \frac{1}{(\alpha + \sqrt{x^2 + y^2})^4} u = f(x, y),$$

where the solution is given by

$$u(x, y) = \sin \left(\frac{1}{\alpha + \sqrt{x^2 + y^2}} \right)$$

and the parameter $\alpha = \frac{1}{10\pi}$ determines the number of oscillations in the solution. The oscillations are clustered near the origin.

Wave front: The Poisson Dirichlet boundary value problem where the solution is given by

$$u(x, y) = \tan^{-1}(50(\sqrt{(x + 0.05)^2 + (y + 0.05)^2} - 0.7)).$$

Figure 7 illustrates the solutions to each of these problems. Table 1 reports the performance of the method for each of these problems with the stopping tolerance set to $\epsilon = 10^{-5}$ and different discretization orders $n_c = 8$ and 16. For all of the experiments the adaptive algorithm achieves the desired tolerance. In fact, for most of the experiments the discretization technique achieves better than the desired tolerance. For both the boundary layer and the locally oscillatory problem resolving the coefficient functions in the PDE is sufficient to resolve the solution. For the wave front problem discretized with the low order basis, the adaptive discretization technique is needed

to achieve the user specified tolerance. For all the experiments, it is computationally beneficial (less expensive to achieve the same or better accuracy) to use a higher order discretization.

Figure 8 illustrates the mesh overlayed on the solution for each experiment. The mesh shows that the method is finding the areas where refinement is necessary. The denseness of the leaf boxes visualize additional the cost of using a low order method.

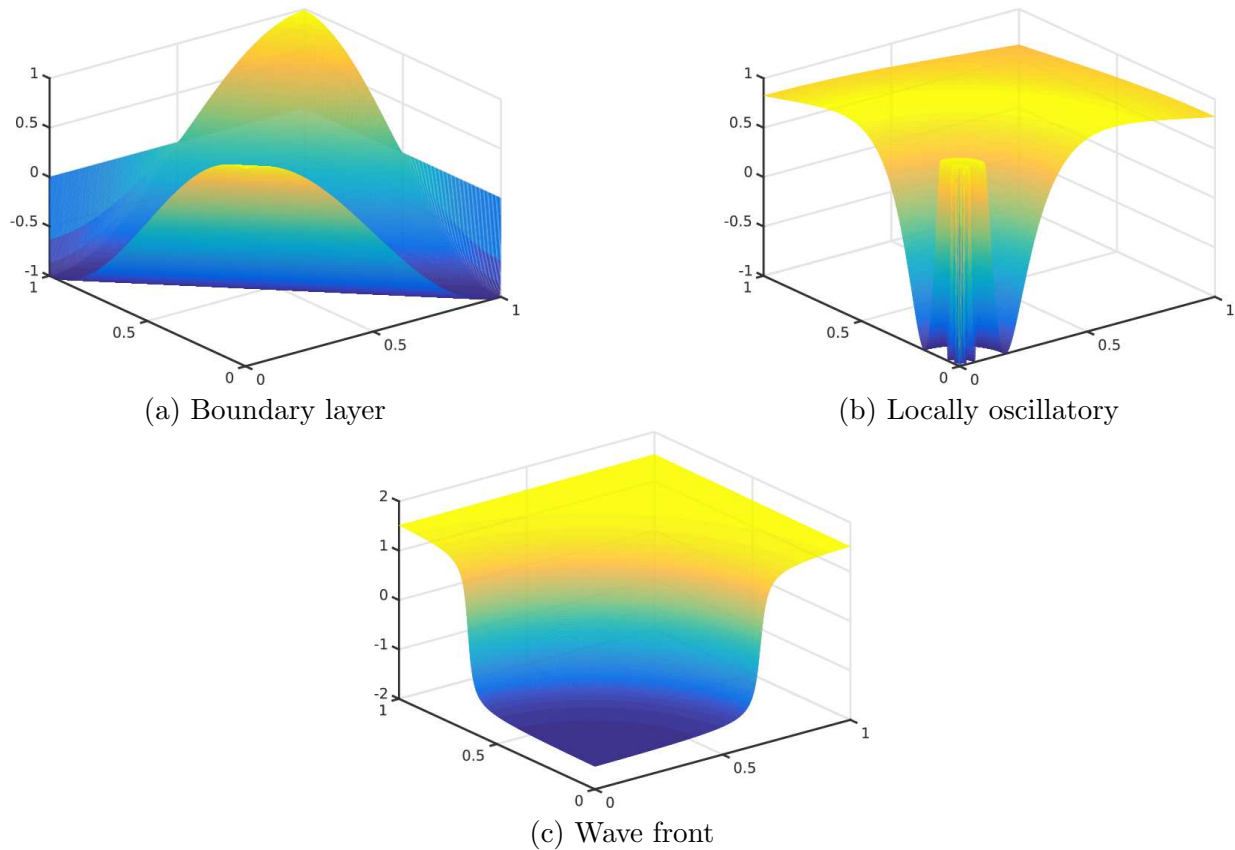


FIGURE 7. Illustration of the solutions to the problems under consideration in section 4.1: (a) Boundary layer problem, (b) Problem with a locally oscillatory solution, and (c) Problem where the solution is a wavefront

Problem	n_c	N_i	N_f	E_{rel}
Boundary layer	8	66610	66610	5.39e-09
	16	2194	2194	7.27e-10
Locally oscillatory	8	21247	21247	1.35e-08
	16	487	487	1.93e-08
Wave front	8	44392	148021	5.43e-04
	16	1405	1405	4.36e-11

TABLE 1. The number of leaf boxes after interpolation N_i , the number of leaf boxes after adaptive interpolation N_f and the average relative error E_{rel} for each of the experiments in section 4.1 with different orders of discretization n_c .

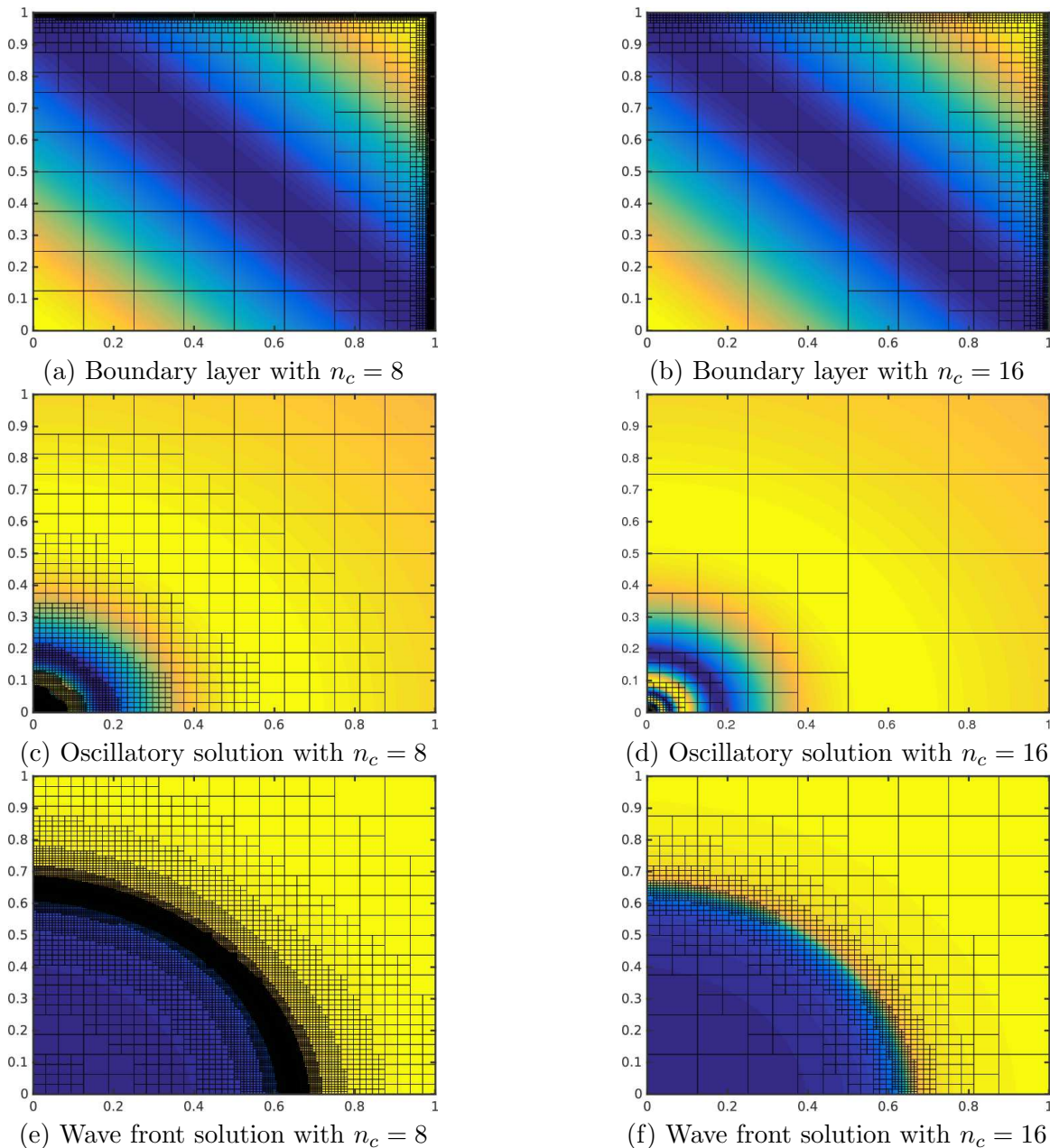


FIGURE 8. Illustration of the mesh generated by the adaptive discretization technique (overlayed on the solution) with $n_c = 8$ and 16 for the problems in section 4.1.

4.2. Problems with unknown solutions. This section illustrates the performance of the adaptive discretization technique when applied two Helmholtz problems of the form

$$-\Delta u - \frac{\omega^2}{(c(\mathbf{x}))^2} u = f(x, y)$$

on $\Omega = (-1, 1)^2$ with a Gaussian source term

$$f(x, y) = \frac{1}{\sqrt{2\pi} \cdot 0.005} e^{-\frac{x^2 + (y - 0.875)^2}{20.005^2}}.$$

Two choices of coefficient function $c(\mathbf{x}) = c(x, y)$ are considered:

Sharp contrast:

$$c(x, y) = \begin{cases} 2.0, & y \geq 0.2 \\ 4.0, & y < 0.2 \end{cases}$$

Smoothly varying

$$c(x, y) = 2 + \frac{2}{1 + e^{200(y-0.2)}}$$

at wave speeds $\omega = 16\pi$ and 32π .

For these problems the solution is unknown. A reference solution is generated by running the uniform refinement scheme until the relative convergence error is less than the stopping tolerance ϵ . This reference solution is then used to generate the relative errors reported in Table 2.

The break in the contrast of the *sharp contrast* experiments is chosen so that it does *not* line up with any boxes thus giving an accurate presentation of the performance of the method for problems with discontinuous media. Since high order accuracy is not possible in this situation, the stopping tolerance was set to $\epsilon = 10^{-3}$. For the smoothly varying media, the tolerance was set $\epsilon = 10^{-5}$.

Table 2 reports on the performance of the method for both choices of contrast at two wave speeds: $\omega = 16\pi$ and $\omega = 32\pi$. The solution is more oscillatory for the larger ω . For these experiments, knowledge of oscillatory behavior of the solution was not exploited. We know that resolving the coefficient functions is not sufficient to achieve the desired accuracy. Thus these examples illustrate the performance of the adaptive discretization technique. Remark 5 explains how to incorporate a priori knowledge of the partial differential equation into the solution technique.

For almost all examples, the method performs as expected. When $\omega = 32\pi$, the low order discretization fails to achieve the desired accuracy. The false positive in convergence of the discretization is the result of using a low order approximation of a highly oscillatory function.

Figure 9 illustrates the mesh generated by the discretization technique when $n_c = 16$ overlaid on the real part of the solution. The discretization is able to pick out the interface whether or not it is smooth. Also the refinement near the interface is the same independent of frequency. This is because the height of that region is small in wave speed. The method is also able to find where there is a change in wave speed around the Gaussian body load. As expected, the solution is approximately twice as oscillatory for $y > 0.2$ and the mesh matches

Remark 5. Using the results from [4], the wave speed could be accounted for a priori by creating a uniform mesh that presets a number of points per wavelength. Then the adaptive procedure can be applied to the resulting uniform mesh.

Problem	ϵ	ω	n_c	N_i	N_f	E_{rel}
Sharp contrast	$1e-3$	16π	8	3130	5218	1.17e-03
			16	3106	3106	3.74e-04
		32π	8	3130	7864	3.39e-03
			16	3106	5194	7.72e-04
Smooth contrast	$1e-5$	16π	8	1372	81568	3.54e-04
			16	238	436	4.30e-06
		32π	8	1372	216169	1.41e-03
			16	238	1012	1.95e-06

TABLE 2. The number of leaf boxes after interpolation N_i , the number of leaf boxes after adaptive interpolation N_f and the average relative error E_{rel} for each of the variable coefficient Helmholtz problems in section 4.2 with different orders of discretization n_c and wave speed ω .

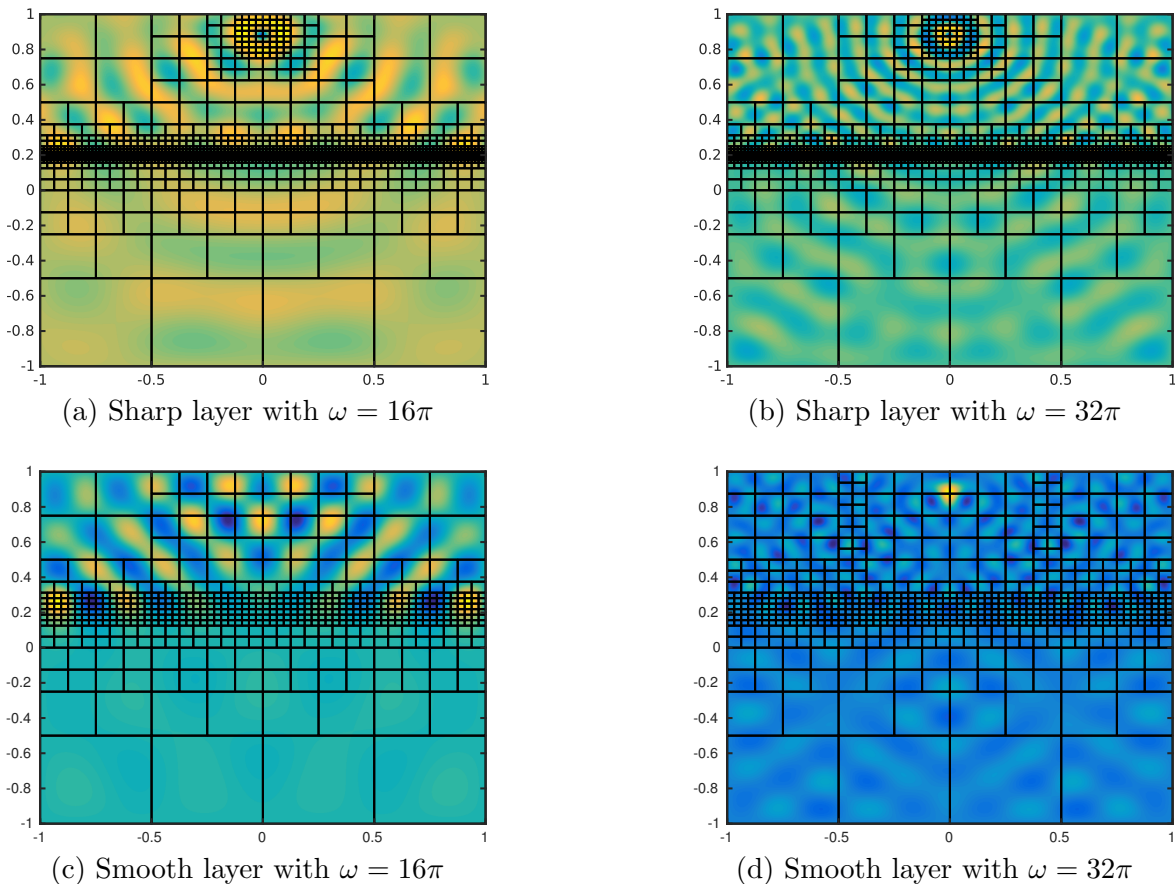


FIGURE 9. Illustration of the mesh generated by the adaptive discretization technique (overlaid on the real part of the solution) with $n_c = 16$ for the problems in section 4.2.

5. CONCLUDING REMARKS

This manuscript presented an high order adaptive discretization technique that comes with an efficient direct solver. The HPS method presented here uses a *new* local pseudospectral discretization that does not involve corner points. By removing the corner points, the leaf computations are less expensive and more stable than the previous version of the method.

The adaptive discretization technique utilizes the modified local tensor product basis to look at convergence of the directional Chebychev expansions to determine which regions of the domain Ω need refinement. Since a discretization is based on decomposing the domain, updating the accompanying direct solver after refinement is inexpensive. The numerical results show that method is able to achieve the user prescribed accuracy and refines only of regions where it is necessary.

6. ACKNOWLEDGEMENTS

The work by A. Gillman is supported by the Alfred P. Sloan foundation and the National Science Foundation (DMS-1522631). The work by P. Geldermans is supported by the National Science Foundation Graduate Research Fellowship under Grant No. 1450681.

REFERENCES

- [1] S. Smith, Lebesgue constants in polynomial interpolation, *Annales Mathematicae et Informaticae* **33** (2006), 109–123.

- [2] T. Babb, A. Gillman, S. Hao, and P.G. Martinsson, An accelerated poisson solver based on a multidomain spectral discretization, In review.
- [3] J. Boyd, Chebyshev and fourier spectral methods, Dover, 2000.
- [4] A. Gillman, A. Barnett, and P.G. Martinsson, A spectrally accurate direct solution technique for frequency-domain scattering problems with variable media, BIT Numerical Mathematics **55** (2015), no. 1, 141–170.
- [5] A. Gillman and P. Martinsson, A direct solver with $o(n)$ complexity for variable coefficient elliptic pdes discretized via a high-order composite spectral collocation method, SIAM Journal on Scientific Computing **36** (2014), no. 4, A2023–A2046, arXiv.org report #1307.2665.
- [6] J.Y. Lee and L. Greengard, A fast adaptive numerical method for stiff two-point boundary value problems, SIAM J. Sci. Comput. **18** (1997), no. 2, 403–429.
- [7] P.G. Martinsson, A direct solver for variable coefficient elliptic pdes discretized via a composite spectral collocation method, Journal of Computational Physics **242** (2013), no. 0, 460 – 479.
- [8] W. F. Mitchell, A collection of 2d elliptic problems for testing adaptive grid refinement algorithms, Applied Mathematics and Computation **220** (2013), 350 – 364.
- [9] L.N. Trefethen, Spectral methods in matlab, SIAM, Philadelphia, 2000.

7. APPENDIX

Consider the variable coefficient Helmholtz impedance boundary value problem

$$(9) \quad \begin{aligned} -\Delta u - \omega^2 c(\mathbf{x})u &= s(x, y) & \mathbf{x} \in \Omega \\ \frac{\partial u}{\partial \nu} + i\eta u &= t(x, y) & \mathbf{x} \in \partial\Omega = \Gamma. \end{aligned}$$

where ν denotes the outward facing normal vector, $c(\mathbf{x})$ is a smooth function, $\omega \in \mathbb{R}$, and $\eta \in \mathbb{C}$.

This section presents the technique for solving variable coefficient Helmholtz problems such as (9) using the HPS method. This technique uses impedance-to-impedance (ItI) operators instead of the DtN operators used in the body of the paper.

Definition 7.1 (impedance-to-impedance map). Fix $\eta \in \mathbb{C}$, and $\mathcal{R} \setminus \eta \neq 0$. Let

$$(10) \quad f := u_n + i\eta u|_{\Gamma}$$

$$(11) \quad g := u_n - i\eta u|_{\Gamma}$$

be Robin traces of u . We refer to f and g as the “incoming” and “outgoing” (respectively) impedance data. For any $\omega > 0$, the *ItI operator* $R : L^2(\Gamma) \rightarrow L^2(\Gamma)$ is defined by

$$(12) \quad Rf = g$$

for f and g the Robin traces of u the solution of (9), for all $f \in L^2(\Gamma)$.

To make the solution technique useful for different choices of $s(x, y)$, we choose to represent the solution u as a superposition of the homogeneous solution w and the particular solution z ; i.e. $u = w + z$ where z is the solution of the following boundary value problem

$$\begin{aligned} -\Delta z - \omega^2 c(\mathbf{x})z &= s(x, y) & \mathbf{x} \in \Omega \\ \frac{\partial z}{\partial \nu} + i\eta z &= 0 & \mathbf{x} \in \partial\Omega = \Gamma \end{aligned}$$

and w is the solution of

$$\begin{aligned} -\Delta w - \omega^2 c(\mathbf{x})w &= 0 & \mathbf{x} \in \Omega \\ \frac{\partial w}{\partial \nu} + i\eta w &= t(x, y) & \mathbf{x} \in \partial\Omega = \Gamma. \end{aligned}$$

Section 7.1 presents the leaf computation and section 7.2 presents the technique for merging two boxes. Throughout the notation is kept consistent with that of section 2. When there is no body load (i.e. $s(x, y) = 0$), the method from [4] is recovered.

7.1. Leaf computation. This section presents the construction of the homogeneous and particular solutions to (9) using the modified spectral collocation method from section 2.1. Additionally, a matrix \mathbf{R} approximating the ItI operator for the homogeneous boundary value problem and the impedance boundary data generated by the particular solution are constructed.

Let \mathbf{N} denote the matrix that takes normal derivatives of the basis functions. Then \mathbf{N} is given by

$$\mathbf{N} = \begin{bmatrix} -\mathbf{D}_x(I_s, I^\tau) \\ \mathbf{D}_y(I_e, I^\tau) \\ \mathbf{D}_x(I_n, I^\tau) \\ -\mathbf{D}_y(I_w, I^\tau) \end{bmatrix}.$$

Then the matrix for creating the incoming impedance data is

$$\mathbf{F} = \mathbf{N} + i\eta \mathbf{I}_{n_c^2}(I_b, I^\tau)$$

and the matrix for creating the outgoing impedance data is

$$\mathbf{G} = \mathbf{N} - i\eta \mathbf{I}_{n_c^2}(I_b, I^\tau)$$

where $\mathbf{I}_{n_c^2}$ is the identity matrix of size n_c^2 .

Then the discretized body load problem to find the approximation to z at the collocation points takes the form

$$(13) \quad \mathbf{B} \begin{bmatrix} \mathbf{z}_b \\ \mathbf{z}_i \end{bmatrix} = \begin{bmatrix} \mathbf{F} \\ \mathbf{A}(i, b) \mathbf{A}(i, i) \end{bmatrix} \mathbf{z} = \begin{bmatrix} \mathbf{0} \\ \mathbf{s} \end{bmatrix}$$

where \mathbf{z} is the vector with the approximate values of z at the collocation points, and \mathbf{s} is $s(x, y)$ evaluated at the interior points.

So the solution operator \mathbf{Y} which gives the approximate particular solution is the solution to

$$\mathbf{B}\mathbf{Y} = \begin{bmatrix} \mathbf{0}_{4n_c-4 \times (n_c-2)^2} \\ \mathbf{I}_{(n_c-2)^2} \end{bmatrix}.$$

Likewise the solution operator $\mathbf{\Psi}$ which give the approximate solution to the homogeneous problem is the solution to

$$\mathbf{B}\mathbf{\Psi} = \begin{bmatrix} \mathbf{I}_{4n_c-4} \\ \mathbf{0}_{(n_c-2)^2 \times 4n_c-4} \end{bmatrix}.$$

To construct the outgoing impedance data from the particular solution \mathbf{h} , the matrix \mathbf{G} needs to be applied to the solution of (13); i.e.

$$\mathbf{h} = \mathbf{G}\mathbf{Y} \begin{bmatrix} \mathbf{0} \\ \mathbf{s} \end{bmatrix} = \mathbf{W} \begin{bmatrix} \mathbf{0} \\ \mathbf{s} \end{bmatrix}.$$

The approximate ItI operator is constructed in the same manner as in [4]. That is

$$\mathbf{R} = \mathbf{G}\mathbf{\Psi}.$$

Putting these together, we find that the outgoing impedance data from the box is given by

$$\mathbf{g} = \mathbf{R}\mathbf{t} + \mathbf{h}$$

where \mathbf{t} is the evaluation of the incoming boundary data function $t(x, y)$ at the points on the boundary.

7.2. Merge two boxes. This section presents the technique for merging two boxes $\Omega^\tau = \Omega^\alpha \cup \Omega^\beta$ for which the ItI matrices and outgoing impedance data from the particular solution has already been computed. In other words, the matrices \mathbf{R}^α and \mathbf{R}^β along with the vectors \mathbf{h}^α and \mathbf{h}^β are available. For consistency, we used the same notation as in [4]. In this section, it is important to remember that unlike the DtN version of the algorithm, the normal derivatives are always pointing exterior to the region they are defined on.

Using the same ordering as in section 2.2, the outgoing impedance data for boxes α and β are given by

$$\begin{bmatrix} \mathbf{g}_1^\alpha \\ \mathbf{g}_3^\alpha \end{bmatrix} = \begin{bmatrix} \mathbf{R}_{11}^\alpha & \mathbf{R}_{13}^\alpha \\ \mathbf{R}_{31}^\alpha & \mathbf{R}_{33}^\alpha \end{bmatrix} \begin{bmatrix} \mathbf{t}_1^\alpha \\ \mathbf{t}_3^\alpha \end{bmatrix} + \begin{bmatrix} \mathbf{h}_1^\alpha \\ \mathbf{h}_3^\alpha \end{bmatrix}; \quad \begin{bmatrix} \mathbf{g}_2^\beta \\ \mathbf{g}_3^\beta \end{bmatrix} = \begin{bmatrix} \mathbf{R}_{22}^\beta & \mathbf{R}_{23}^\beta \\ \mathbf{R}_{32}^\beta & \mathbf{R}_{33}^\beta \end{bmatrix} \begin{bmatrix} \mathbf{t}_2^\beta \\ \mathbf{t}_3^\beta \end{bmatrix} + \begin{bmatrix} \mathbf{h}_2^\beta \\ \mathbf{h}_3^\beta \end{bmatrix}$$

where $\begin{bmatrix} \mathbf{h}_1^\alpha \\ \mathbf{h}_3^\alpha \end{bmatrix}$ and $\begin{bmatrix} \mathbf{h}_2^\beta \\ \mathbf{h}_3^\beta \end{bmatrix}$ are the outgoing impedance data due to the particular solutions on each box.

Since the normal vectors are opposite in each box, we know $\mathbf{t}_3^\alpha = -\mathbf{g}_3^\beta$ and $\mathbf{g}_3^\alpha = -\mathbf{t}_3^\beta$. Using this information in the bottom row equations, \mathbf{t}_3^α and \mathbf{t}_3^β can be found in terms of \mathbf{t}_1^α , \mathbf{t}_2^β , \mathbf{h}_3^α , and \mathbf{h}_3^β . They are given by

$$(14) \quad \mathbf{t}_3^\alpha = \mathbf{W}^{-1} \left[\mathbf{R}_{33}^\beta \mathbf{R}_{31}^\alpha - \mathbf{R}_{32}^\beta \right] \begin{bmatrix} \mathbf{t}_1^\alpha \\ \mathbf{t}_2^\beta \end{bmatrix} + \mathbf{W}^{-1} \left(\mathbf{R}_{33}^\beta \mathbf{h}_3^\alpha - \mathbf{h}_3^\beta \right)$$

and

$$(15) \quad \mathbf{t}_3^\beta = \left[-\mathbf{R}_{31}^\alpha - \mathbf{R}_{33}^\alpha \mathbf{W}^{-1} \mathbf{R}_{33}^\beta \mathbf{R}_{31}^\alpha \mid \mathbf{R}_{33}^\alpha \mathbf{W}^{-1} \mathbf{R}_{32}^\beta \right] \begin{bmatrix} \mathbf{t}_1^\alpha \\ \mathbf{t}_2^\beta \end{bmatrix} - \left(\mathbf{I} + \mathbf{R}_{33}^\alpha \mathbf{W}^{-1} \mathbf{R}_{33}^\beta \right) \mathbf{h}_3^\alpha + \mathbf{R}_{33}^\alpha \mathbf{W}^{-1} \mathbf{h}_3^\beta$$

where $\mathbf{W} = \mathbf{I} - \mathbf{R}_{33}^\beta \mathbf{R}_{33}^\alpha$.

Plugging (14) and (15) into the top row equations results in the following expression for the outgoing impedance data for the box $\Omega^\alpha \cup \Omega^\beta$

$$(16) \quad \begin{bmatrix} \mathbf{g}_1^\alpha \\ \mathbf{g}_2^\beta \end{bmatrix} = \begin{bmatrix} \mathbf{R}_{11}^\alpha + \mathbf{R}_{13}^\alpha \mathbf{W}^{-1} \mathbf{R}_{33}^\beta \mathbf{R}_{31}^\alpha & -\mathbf{R}_{13}^\alpha \mathbf{W}^{-1} \mathbf{R}_{32}^\beta \\ -\mathbf{R}_{23}^\beta \left(\mathbf{R}_{31}^\alpha + \mathbf{R}_{33}^\alpha \mathbf{W}^{-1} \mathbf{R}_{33}^\beta \mathbf{R}_{31}^\alpha \right) & \mathbf{R}_{22}^\beta + \mathbf{R}_{23}^\beta \mathbf{R}_{33}^\alpha \mathbf{W}^{-1} \mathbf{R}_{32}^\beta \end{bmatrix} \begin{bmatrix} \mathbf{t}_1^\alpha \\ \mathbf{t}_2^\beta \end{bmatrix} \\ + \begin{bmatrix} \mathbf{h}_1^\alpha \\ \mathbf{h}_2^\beta \end{bmatrix} + \begin{bmatrix} \mathbf{R}_{13}^\alpha \mathbf{W}^{-1} \left(\mathbf{R}_{33}^\beta \mathbf{h}_3^\alpha - \mathbf{h}_3^\beta \right) \\ -\mathbf{R}_{23}^\beta \left(\mathbf{I} + \mathbf{R}_{33}^\alpha \mathbf{W}^{-1} \mathbf{R}_{33}^\beta \right) \mathbf{h}_3^\alpha + \mathbf{R}_{23}^\beta \mathbf{R}_{33}^\alpha \mathbf{W}^{-1} \mathbf{h}_3^\beta \end{bmatrix} \\ = \mathbf{R}^\tau \begin{bmatrix} \mathbf{t}_1^\alpha \\ \mathbf{t}_2^\beta \end{bmatrix} + \begin{bmatrix} \hat{\mathbf{h}}_1^\alpha \\ \hat{\mathbf{h}}_2^\beta \end{bmatrix}$$

7.3. The full algorithm. As with the homogeneous DtN solution technique, the solver can be broken into the precomputation and the solve phase. The precomputation for a leaf box τ is similar to before except now a solution operator \mathbf{Y}^τ yielding the particular solution on τ and a matrix \mathbf{W} giving the outgoing particular impedance data are constructed. Also, instead of a DtN matrix, an ItI matrix is constructed. The precomputation for a box τ with children α and β is more intense. A collection of operators giving the incoming impedance data on the shared edge are constructed from the incoming impedance data from τ and the outgoing impedance particular solution data (which is not yet computed) on that edge from both α and β . Thus a collection of operators for constructing the outgoing particular solution on the shared edge are constructed as well as the operators needed to construct the outgoing impedance particular solution data on the boundary of τ . Notice looking

the formulas (14), (15) and (16) there is significant overlap in computation thus keeping the cost and memory of the precomputation in check.

The solve step sweeps the tree twice (instead of once as in the homogeneous solver). First, starting from the leaf boxes moving up the tree to Ω^1 , the outgoing impedance particular solution data are constructed. Then using this information along with the boundary condition on Ω , the incoming impedance boundary data is propagated from the top of the tree down to the leaf boxes.